nature physics

ARTICLES

PUBLISHED ONLINE: 8 JULY 2012 | DOI: 10.1038/NPHYS2356

A wideband, low-noise superconducting amplifier with high dynamic range

Byeong Ho Eom[1], Peter K. Day[2]*, Henry G. LeDuc[2] and Jonas Zmuidzinas[1,2]

An ideal amplifier has very low noise, operates over a broad frequency range, and has large dynamic range. Unfortunately, it is difficult to obtain all of these characteristics simultaneously. For example, modern transistor amplifiers offer multi-octave bandwidths and excellent dynamic range, but their noise remains far above the limit set by the uncertainty principle of quantum mechanics. Parametric amplifiers can reach the quantum-mechanical limit, but generally are narrow band and have very limited dynamic range. Here we describe a parametric amplifier that overcomes these limitations through the use of a travelling-wave geometry and the nonlinear kinetic inductance of a superconducting transmission line. We measure gain extending over 2 GHz on either side of an 11.56 GHz pump tone and place an upper limit on the added noise of 3.4 photons at 9.4 GHz. The dynamic range is very large, and the concept can be applied from gigahertz frequencies to ~1 THz.

Over the past decade, the combination of high-performance superconducting microresonators and low-noise, microwave frequency cryogenic transistor amplifier readouts has proven to be particularly powerful for a wide range of applications, including photon detection and quantum information experiments[1–3]. These developments have generated a strong renewed interest in superconducting amplifiers that achieve even lower readout noise[4–9]. Most of these devices are parametric amplifiers (paramps) that make use of the nonlinear inductance of the Josephson junction, which is almost ideally reactive with little dissipation below the critical current I_c. As a result, Josephson paramps[10,11] can be exquisitely sensitive, approaching the standard quantum limit of half a photon $\hbar\omega/2$ of added noise power per unit bandwidth in the standard case when both quadratures of a signal at frequency ω are amplified equally[12]. Even less noise is possible in situations when only one quadrature is amplified[13]. In comparison, the added noise of cryogenic transistor amplifiers is typically 10–20 times the quantum limit[14]. However, the dynamic range of Josephson paramps is regulated by the Josephson energy $E_J = \hbar I_c/2e$ (e is the electron charge) to values that are far lower than for transistor amplifiers. Furthermore, as in optical parametric oscillators in which light passes many times through a nonlinear medium, previous superconducting paramps generally use resonant circuits to enhance the effective nonlinearity and thus achieve high gain. Consequently, amplification is achieved over a narrow instantaneous frequency range, typically of the order of a few megahertz, versus ~10 GHz for transistor amplifiers. This results in a relatively slow response time, which can hinder observation of time-dependent phenomena, for example quantum jumps[15]. Also, as with superconducting quantum interference devices[16], the combination of a limited dynamic range and a limited bandwidth results in a low Shannon information capacity and limits the utility of Josephson paramps for multiplexed readout of detector arrays[17].

Instead of using a resonator, the optical or electrical path may be unfolded into a long nonlinear transmission line or waveguide. This results in a travelling wave paramp[18,19] which has a very broad intrinsic bandwidth. However, a low-dissipation medium that is sufficiently nonlinear over a realizable length must be found. At visible and infrared wavelengths, these requirements are met in optical fibres[20] and silicon waveguides[21] through the nonlinear process of four-wave mixing (FWM) that results from the intensity dependence of the refractive index, that is the Kerr effect. Fibre paramps achieve high (>60 dB) gain[20] and single-quadrature versions have exhibited noise levels below the standard quantum limit[22]. An analogous microwave device using a metamaterial of numerous Josephson junctions embedded in a transmission line[23,24] has been proposed and investigated, but this design has not yet resulted in a practical amplifier.

Like a Josephson junction, a thin superconducting wire behaves as a nondissipative inductor for currents below a critical current I_c. The critical current is therefore an obvious scale for nonlinear behaviour in both junctions and wires, although I_c for a wire is typically orders of magnitude larger than for a junction. Indeed, the phenomenological Ginzburg–Landau theory and the microscopic Bardeen-Cooper-Schrieffer (BCS) theory[25,26] both predict the nonlinearity of the kinetic inductance of superconductors. In practice this nonlinearity is usually weak, although resonant paramps based on this effect have been proposed and investigated[27,28]. Here we show that the use of a high-resistivity superconductor, such as TiN (ref. 29) or NbTiN, results in a kinetic inductance nonlinearity that is sufficient to allow parametric gain in a practical, realizable travelling wave geometry.

The current variation of the kinetic inductance of a superconducting wire is expected to be quadratic to lowest order, that is $L_k(I) \approx L_k(0)[1 + (I/I_*)^2]$ for $I/I_* \ll 1$, just as in the case of Josephson junctions. I_* sets the scale of the nonlinearity. The Mattis–Bardeen theory[30] gives $L_k(0) = \hbar R_n/\pi\Delta$ for a wire with normal state resistance R_n and superconducting gap parameter Δ, whose transverse dimensions are small enough so that the current distribution is approximately uniform. I_* is comparable to I_c, and can be roughly estimated by equating the kinetic energy of the Cooper pairs $L_k I^2/2$ to the pairing energy $E_p = 2N_0\Delta^2 V$, where N_0 is the density of states at the Fermi level and V is the volume. The resulting expression for I_*^2 is proportional to $1/R_n$. The phase velocity of the transmission line is $v_{ph} = 1/\sqrt{\mathcal{LC}} \approx v_{ph}(0)(1 - \alpha I^2/2I_*^2)$, where $\mathcal{L}$ and $\mathcal{C}$ are the total inductance and capacitance per unit

[1]California Institute of Technology, Pasadena, California 91125, USA, [2]Jet Propulsion Laboratory, California Institute of Technology, Pasadena, California 91109, USA. *e-mail: Peter.K.Day@jpl.nasa.gov.

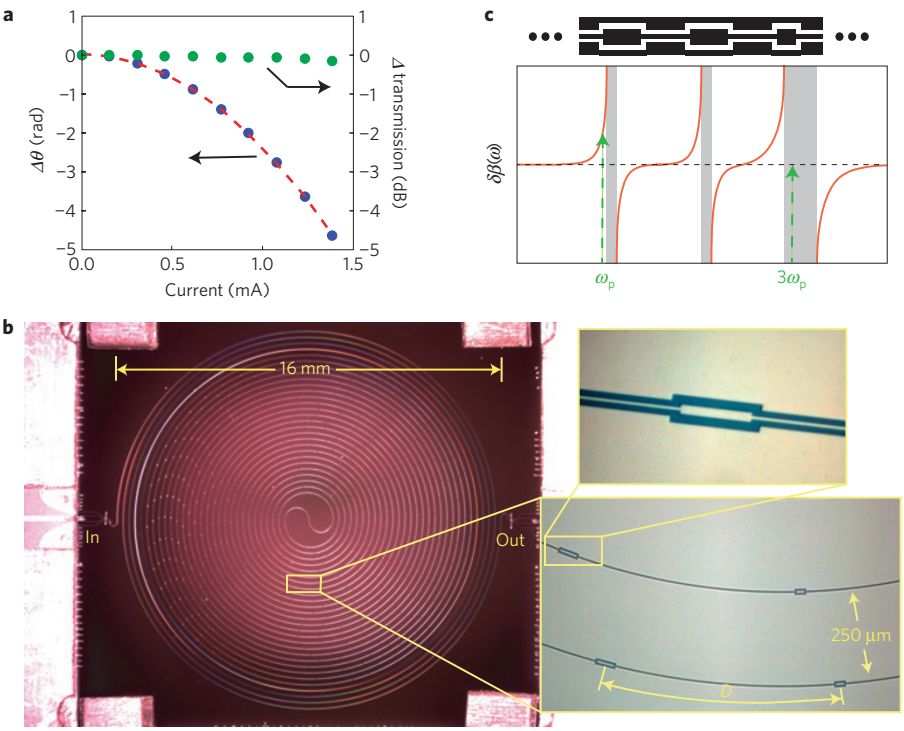

Figure 1 | Response to d.c. current and amplifier design. a, Plot illustrating the nonlinearity of the kinetic inductance. A NbTiN CPW transmission line (shown in **b**) was measured in transmission using a microwave network analyser. The total phase length was 670 rad at 4 GHz. Using bias tees, a d.c. current was passed down the centre conductor. The resulting microwave phase shift measured at 4 GHz (blue dots) exhibits a quadratic dependence (red dashed line) with current. No comparable effect occurred when adjusting the voltage of the centre strip relative to the ground planes. This shows that the kinetic inductance has a nonlinear behaviour that is described well by $\delta L_{kin} \propto I^2$. The dissipative change (green dots) is <0.15 dB. **b**, A picture of the amplifier (left) which consists of a 0.8 m length of NbTiN CPW line arranged in a double spiral to reduce resonances due to coupling between adjacent lines[35]. The thickness of the line is 35 nm and the centre conductor and gap widths are 1 μm. At the input and output of the line, the CPW geometry tapers from centre strip and gap widths of 30 and 5 μm to adiabatically transform the characteristic impedance of the line from 50 to 300 Ω. The line is periodically loaded by widening a short section after every length $D = 877$ μm, as shown on the right, producing the stop band and dispersion characteristics. The phase velocity on the line is $0.1c$, where c is the speed of light, owing to its large kinetic inductance. **c**, An illustration of the effect of the periodic loading pattern (shown schematically) on the transmission of an infinite transmission line. The grey regions represent stop bands; waves in these frequency ranges decay evanescently. The graph represents the difference between the propagation constant of the line and linear ($\propto\omega$) dispersion. As the fractional width of the third stop band is much larger than the first, the pump can be placed at a propagating frequency while $3\omega_p$ is blocked.

length, and α is the ratio of kinetic inductance to total inductance. The magnitude of the Kerr effect in the line is therefore proportional to α/I_*^2 and is enhanced in films with high normal state resistivity ρ_n owing both to large α and small I_*. The TiN and NbTiN films produced in our laboratory have $\rho_n \approx 100$ μΩ cm, nearly three orders of magnitude larger than for typical aluminium films, and have very low microwave loss in the superconducting state[29]. The high resistivity also results in a large penetration depth λ, which increases in inverse proportion to the square root of the mean free path in the extreme dirty limit. The screening length for magnetic fields perpendicular to the film is λ^2/d (ref. 31) and reaches 2–20 μm depending on thickness ($d \sim 20$–50 nm typically) and critical temperature T_c; so a uniform current density is readily achieved in our micrometre-scale wires patterned by optical lithography.

The nonlinear kinetic inductance is illustrated in Fig. 1, which shows the phase shift of a microwave tone passing through a NbTiN transmission line as a function of the d.c. current flowing through it. The coplanar waveguide (CPW) transmission line was patterned from a single NbTiN film deposited on an unoxidized, high resistivity silicon substrate. In fact, such a current-controlled phase shifter has been previously proposed[32] but not successfully demonstrated, owing to an increase in the microwave dissipation with d.c. current. Similar dissipative behaviour has also been noted in superconducting thin-film resonators (see Supplementary Information). In contrast, only a very modest (<0.15 dB) increase in dissipation was observed for the range of phase shifts shown in Fig. 1. Also, provided that the temperature is kept well below the critical temperature T_c, our TiN (ref. 29) and NbTiN microresonators remain nondissipative for microwave currents sufficiently strong to develop a significant reactive nonlinearity. These results are described in the Supplementary Information.

The parametric gain produced through FWM can be calculated using coupled mode equations that have been developed to describe optical fibre paramps (see Supplementary Information). In general, FWM may involve two separate pump tones, but we consider only the degenerate case where the pump frequencies are equal. The equations then describe the interaction of the pump at angular frequency $\omega_p = 2\pi f_p$, signal at ω_s, and the generated idler tone at $\omega_i = 2\omega_p - \omega_s$. For a dispersionless line, which is a good approximation for a uniform superconducting transmission line at frequencies well below the gap frequency $2\Delta/h$, the signal and idler gains for $f_s \approx f_p$ are $G_s = 1 + (\Delta\theta)^2$ and $G_i = (\Delta\theta)^2$, where $\Delta\theta$ is the nonlinear phase shift, in radians, of the pump tone due to its own a.c. current. Figure 1 shows that phase shifts of several radians can be achieved in response to a d.c. current. Comparable phase shifts can also be achieved in response to microwave currents, as described in the Supplementary Information. Dispersion, due either to material or waveguide properties, controls the phase slippage between the waves as they propagate, which in turn determines whether the signal is amplified

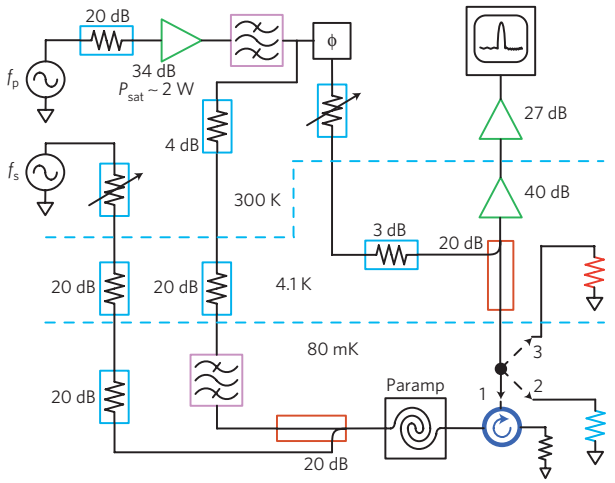

Figure 2 | Circuit for paramp gain and noise measurements. The pump tone is produced by a low phase noise synthesizer (<150 dBc at 10 MHz offset), amplified to a suitable level and filtered using a copper cavity mode bandpass filter. After a splitter, the pump tone is attenuated at 4 K and filtered using a commercial combline filter with a bandwidth of 200 MHz around 11.56 GHz. This bandpass filter is used for the noise measurements, and provides greater than 70 dB of attenuation for noise on the pump line at the signal frequencies of interest. The other output of the splitter is adjusted in phase and amplitude and used to null the pump tone that passes through the paramp and would otherwise saturate the 4 K HEMT amplifier. The signal tone is generated either with another synthesizer or a vector network analyser. Its level is reduced by warm and cold attenuators and coupled to the paramp input using a 20 dB directional coupler on the base temperature stage of the dilution refrigerator. A cryogenic isolator is used after the paramp to absorb noise radiated towards the paramp by the HEMT post-amplification stage. The noise of the paramp and HEMT is measured with the help of a cryogenic switch after the isolator, which can connect the HEMT amplifier to either the paramp or 50 Ω loads at the base temperature and 4 K stages. The loss of the isolator was measured to be 0.8 dB. The switch has negligible loss. After further amplification at room temperature, the signal is measured using either a spectrum analyser or the network analyser. The diagram does not include coax line losses. All coaxes below 4 K are superconducting.

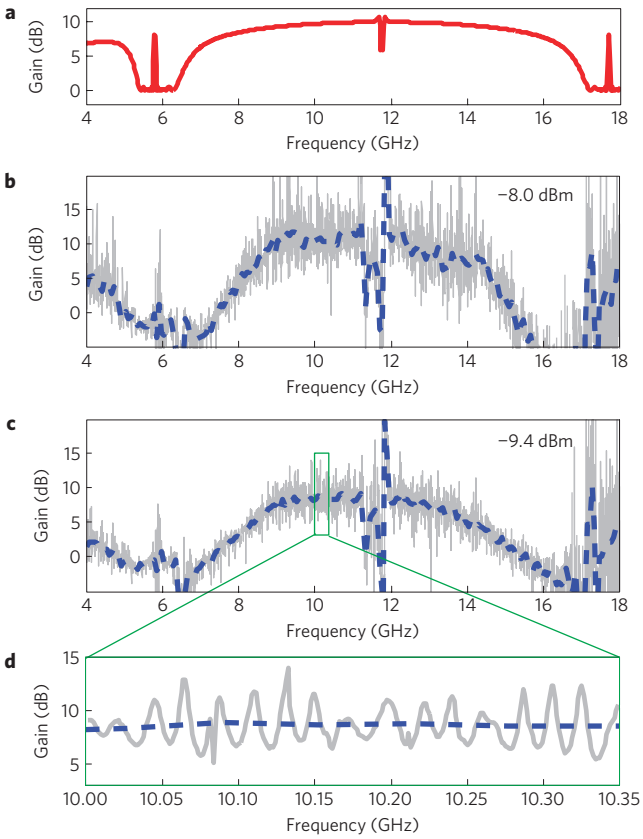

Figure 3 | Measured and calculated gain. a, This plot shows a gain profile calculated using the coupled mode equations for FWM including the dispersion of the device determined using a transmission line model of the periodic loading structure. A parameter quantifying the nonlinearity of the line and the frequency shift of the dispersion curve due to the cross-phase modulation from the pump tone were adjusted for a reasonable match to the data. **b**,**c**, These plots show the measured ratio of 'pump on' over 'pump off' transmission (grey lines) for two pump powers (−8.0 and −9.4 dBm at the input of the paramp). The blue dashed lines are the measured data smoothed by averaging over 60 MHz. The large peak at 11.9 GHz is an artefact arising from the shift to lower frequency of the transmission dip produced by the periodic loading. **d**, The spacing between the gain ripples, shown on an expanded scale, corresponds to the electrical length of the NbTiN transmission line.

or deamplified. The linear dispersion $\Delta\beta = \beta(\omega_s) + \beta(\omega_i) - 2\beta(\omega_p)$ involves a difference of the propagation constants $\beta(\omega)$ for small-amplitude waves at the signal, idler and pump frequencies, and vanishes for a dispersionless line obeying $\beta(\omega) = \omega/v_{ph}$, with frequency independent v_{ph}. The coupled mode equations predict that maximum gain occurs when $\Delta\beta = -2\Delta\theta/L$ because this value of linear dispersion compensates for the phase slippage that arises from the nonlinearity. Furthermore, the resulting gain $G_s = \exp(2\Delta\theta)/4$ varies exponentially with line length L rather than quadratically[20,33]. For much larger or smaller values of $\Delta\beta$, loss of phase match yields low gain.

In fact, some amount of dispersion is necessary, because a dispersionless Kerr medium leads to generation of a shock front when $\Delta\theta \gtrsim 1$, preventing significant parametric gain[34]. Indeed, a superconducting line generates the third harmonic $3f_p$ due to the voltage term $I^2 dI/dt$ arising from the nonlinear inductance. This is the first step in the formation of the shock front: once the $3f_p$ harmonic is present, other harmonics can be generated. This problem is dealt with in a simple manner using dispersion engineering, leading to the device shown in Fig. 1. Periodic perturbations are included in the CPW transmission line with a separation corresponding to half of a wavelength at frequency f_{per}, with f_{per} slightly larger than $3f_p$. Much like an electronic or photonic bandgap, this results in a stop band centred at f_{per} that includes $3f_p$, blocking harmonic generation. We also slightly alter every third perturbation, resulting in weak stop bands around $f_{per}/3$ and $2f_{per}/3$ (Fig. 1c). This gives rise to localized dispersion features near these frequencies; fine-tuning of the pump frequency f_p in the vicinity of these features allows the optimum value of $\Delta\beta$ to be achieved for a wide range of signal frequencies. For the device shown in Fig. 1, the stop bands occur at multiples of $f_{per}/3 \approx 5.9$ GHz, not far from the design value of 5 GHz. We chose to operate the device with the pump tuned near $2f_{per}/3 \approx 11.8$ GHz because this dispersion feature was stronger; note that a strong stop band also occurs at 3×11.8 GHz, which prevents formation of pump harmonics.

We measured the gain of the amplifier with the pump tuned to 11.56 GHz using the circuit shown in Fig. 2, excluding the bandpass filter. The gain increases with pump power until a critical pump power is reached, which we identify with the onset of nonlinear dissipation in the line. Significant gain is observed over a frequency range of approximately 8–14 GHz, with a notch around the pump frequency (Fig. 3). A theoretical gain curve (Fig. 3, top), generated by integrating the coupled mode equations and including a model of the loaded line dispersion

(see Supplementary Information), is in rough agreement with the average gain. However, there is a fine-scale variation of the gain, which is approximately periodic with signal frequency, with a gain ripple that increases with pump power and has a divergent behaviour around the critical pump power. The average gain at the higher pump power shown is 10 dB, with several peaks extending above 20 dB. From the frequency spacing, it is clear that the gain ripple is due to standing waves created by reflections at the ends of the line. The reflections are probably caused by the non-optimal on-chip tapered impedance transformers, or possibly the wirebond transitions or other components near the device. For pump frequencies much different from 11.56 GHz, the maximum achievable gain is only on the order of a few dB, confirming the role of the dispersion engineering in the operation of the amplifier.

To measure the noise of the paramp, we chose signal frequencies corresponding to gain peaks. For example, at $f_s = 9.37$ GHz the gain was 18.6 dB. The output power of the amplifier chain was measured in a narrow band around f_s using a spectrum analyser. A cryogenic switch (Fig. 2) was used to calibrate the system. The added noise power per unit bandwidth of the high electron mobility transistor (HEMT) at 4.1 K was measured to be $A_{HEMT} = 16.1$, in photon units ($\hbar\omega$), by switching between between 50 Ω resistors on the 4.1 K and base temperature stages of the dilution refrigerator (switch positions 2 and 3). With the paramp connected to the HEMT (position 1), we make measurements with the pump tone both on and off (Fig. 4). Because the gain peak shifts to lower frequency when the pump is applied, we slightly reduce the signal frequency to remain at the peak. As the transmission of the measurement system should remain constant over this small frequency interval, the increase in the output signal power gives the gain of the paramp, $G_{PA} = 18.6$ dB. At 9.37 GHz, it is evident that the paramp is considerably less noisy than the HEMT, because the signal-to-noise ratio improves by 7.8 dB with the pump turned on (Fig. 4). The paramp noise may be quantitatively determined from the ratio $R = (n_{on} - n_0)/(n_{off} - n_0)$, where n_{on} and n_{off} are the measured noise levels with pump on and off, and n_0 is the noise from sources after the HEMT, which is found by turning off the HEMT. However, with the paramp connected to the HEMT (switch position 1) and no pump applied, we find that the noise floor is slightly higher than with the HEMT connected to the cold load. This increase in the system added noise is $A_{sys} = 2.9$. We have not yet determined the origin of this noise; therefore, we do not know the gain G_{sys} this noise experiences when the pump is turned on. As a result, when we calculate the noise added by the paramp

$$A_{PA} = \frac{R-1}{G'_{PA}} A_H + \frac{R - G_{sys}}{G'_{PA}} A_{sys} + \frac{R}{2G'_{PA}} - \frac{1}{2} \quad (1)$$

we obtain a range of values $1.1 \leq A_{PA} \leq 3.4$, corresponding to $1 \leq G_{sys} \leq G'_{PA}$. Here G'_{PA} accounts for the isolator loss (Fig. 2).

To confirm the noise measurement, we used a variable-temperature 50 Ω resistor connected to the paramp input through a 3 dB hybrid coupler (Fig. 4). The slope of the linear relationship between output noise and resistor temperature calibrates the gain of the system, and extrapolating this relationship to zero resistor temperature gives the added noise of the amplifier plus any further input noise. If we assume that only vacuum noise $\hbar\omega/2$ is present at the input, the added noise of the paramp is 3.3 ± 0.2 photons, in agreement with the previous measurement. Using different gain peaks, the noise was measured at other frequencies. Closer to the pump frequency, the noise was observed to increase to between 4 and 5 photons. Very close to the pump frequency, the noise would be expected to rise as the pump phase noise is not adequately suppressed by the filters (Fig. 2). At 8.93 GHz the noise was 2.3 photons, but the gain was only 12.5 dB.

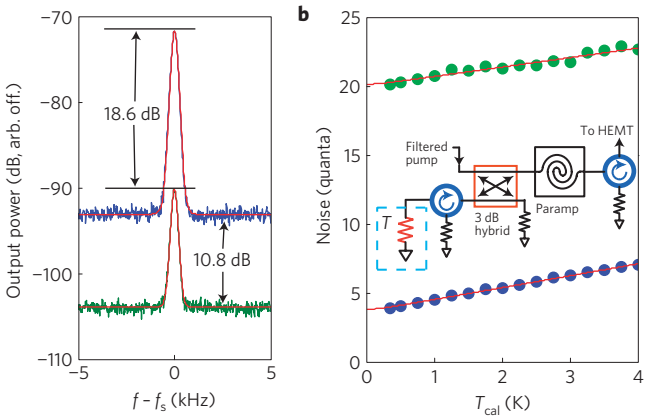

Figure 4 | Noise compared with the HEMT amplifier. a, Increase in signal-to-noise ratio of a weak microwave tone applied to the input of the paramp. With the pump off (green) the noise floor is limited by the HEMT amplifier. With the pump on (blue) the signal gain is 18.6 dB and signal-to-noise ratio has increased by 7.8 dB. The red lines are a fit to the spectrum analyser's response to a monochromatic signal. The 'pump on' data were taken with $f_s = 9.3672$ GHz, while the 'pump off' data used $f_s = 9.3845$ GHz. **b**, Noise referred to the input of the paramp (blue) and the HEMT amplifier (green) in photon units versus the calibrator temperature. The circuit configuration for this measurement is shown in the inset. The 50 Ω resistor is mounted on a temperature-controlled stage, connected to the mixing chamber, and terminates a 0.85 mm diameter NbTi coax line. The noise signal is added to the pump at the input of the paramp using a 3 dB hybrid coupler. The total loss between the resistor and the paramp input was 4.1 ± 0.5 dB, where we have taken the insertion loss of the hybrid to lie between the room temperature measured value of 1 dB and zero. An isolator is used between the noise calibrator and the hybrid to avoid heating from reflected pump power.

The dynamic range of the paramp was investigated with the cryogenic HEMT amplifier removed from the system, as it was found that the gain compression point of the HEMT would be reached before that of the paramp. At 11.05 GHz and 28 dB signal gain, the gain compressed by 1 dB for a signal power of −62 dBm. At 9.43 GHz and 18 dB signal gain, the 1 dB compression point was at −52 dBm. Using the noise measured with the HEMT post-amplifier, as described above, the noise power in a 1 Hz bandwidth was 4.7 and $3.4\hbar\omega$ near 11.05 and 9.43 GHz, respectively. The ratio of the maximum signal power to the noise in a 1 Hz bandwidth is then 134 dB at 28 dB gain and 144 dB at 18 dB gain (see Supplementary Information for further details). Theoretically, saturation of the paramp occurs when the amplified signal power becomes a significant fraction of the pump power, around 100 μW for this device, so that the pump becomes depleted.

In summary, we have demonstrated a simple and robust superconducting amplifier with very low noise, wide bandwidth, and high dynamic range. In fact, given the extremely low dissipation of the superconductors used[29], it seems likely that the amplifier is operating very near the quantum limit and that the added noise is due to imperfections of the present measurement system. For example, the image frequency $f_i = 13.75$ GHz is outside the bandwidth of our isolator, so noise from the HEMT may leak back towards the paramp at that frequency and contribute to noise at f_s. Design improvements should allow high (>20 dB) gain to be achieved over an octave of instantaneous bandwidth. The amplifier is straightforward to fabricate, consisting only of a patterned metal film on a dielectric substrate. Periodic loading structures can readily be designed for operating frequencies in the microwave, millimetre-wave, and submillimetre-wave bands, potentially approaching the gap frequency of the superconducting film ($2\Delta/h \approx 1.4$ THz for

NbTiN). The lower frequency limit is determined only by the length of transmission line that can be fabricated. By applying a d.c. current bias, we observed idler generation at $\omega_p - \omega_s$, suggesting that the amplifier could also be operated in a three-wave mixing mode if the dispersion were engineered to produce a stop band at $2\omega_p$. More generally, we hope that our demonstration will serve as a clear illustration of the remarkable nonlinear properties of highly resistive superconductors and will stimulate development of a much broader set of applications, just as was the case for nonlinear optics.

Received 4 April 2012; accepted 1 June 2012; published online 8 July 2012

References

1. Day, P. K., LeDuc, H. G., Mazin, B. A., Vayonakis, A. & Zmuidzinas, J. A broadband superconducting detector suitable for use in large arrays. *Nature* **425,** 817–821 (2003).
2. Wallraff, A. *et al.* Strong coupling of a single photon to a superconducting qubit using circuit quantum electrodynamics. *Nature* **431,** 162–167 (2004).
3. Zmuidzinas, J. Superconducting microresonators: Physics and applications. *Annu. Rev. Condens. Matter Phys.* **3,** 169–214 (2012).
4. Castellanos-Beltran, M. A., Irwin, K. D., Hilton, G. C., Vale, L. R. & Lehnert, K. W. Amplification and squeezing of quantum noise with a tunable Josephson metamaterial. *Nature Phys.* **4,** 929–931 (2008).
5. Yamamoto, T. *et al.* Flux-driven Josephson parametric amplifier. *Appl. Phys. Lett.* **93,** 042510 (2008).
6. Bergeal, N. *et al.* Phase-preserving amplification near the quantum limit with a Josephson ring modulator. *Nature* **465,** 64–68 (2010).
7. Spietz, L., Irwin, K., Lee, M. & Aumentado, J. Noise performance of lumped element direct current superconducting quantum interference device amplifiers in the 4–8 GHz range. *Appl. Phys. Lett.* **97,** 142502 (2010).
8. Hover, D. *et al.* Superconducting low-inductance undulatory galvanometer microwave amplifier. *Appl. Phys. Lett.* **100,** 063503 (2012).
9. Mück, M., Kycia, J. B. & Clarke, J. Superconducting quantum interference device as a near-quantum-limited amplifier at 0.5 GHz. *Appl. Phys. Lett.* **78,** 967–969 (2001).
10. Zimmer, H. Parametric amplification of microwaves in superconducting Josephson tunnel junctions. *Appl. Phys. Lett.* **10,** 193–195 (1967).
11. Moshovich, R. *et al.* Observation of zero-point noise squeezing via a Josephson parametric amplifier. *Phys. Rev. Lett.* **65,** 1419–1422 (1990).
12. Louisell, W. H., Yariv, A. & Siegman, A. E. Quantum fluctuations and noise in parametric processes. I. *Phys. Rev.* **124,** 1646–1654 (1961).
13. Caves, C. M. Quantum limits on noise in linear amplifiers. *Phys. Rev. D* **26,** 1817–1839 (1982).
14. Pospieszalski, M. W. Extremely low-noise amplification with cryogenic FETs and HFETs: 1970–2004. *IEEE Microw. Mag.* **6,** 62–75 (2005).
15. Vijay, R., Slichter, D. H. & Siddiqi, I. Observation of quantum jumps in a superconducting artificial atom. *Phys. Rev. Lett.* **106,** 110502 (2011).
16. Clarke, J. & Braginski, A. I. *The SQUID Handbook: Fundamentals and Technology of SQUIDs and SQUID Systems* 1st edn (Wiley-VCH, 2004).
17. Irwin, K. D. in *AIP Conf. Proc.* (eds Young, B., Cabrera, B. & Miller, A.) 229–236 (American Institute of Physics Conference Series, Vol. 1185, 2009).
18. Cullen, A. L. A travelling-wave parametric amplifier. *Nature* **181,** 332 (1958).
19. Tien, P. K. Parametric amplification and frequency mixing in propagating circuits. *J. Appl. Phys.* **29,** 1347–1357 (1958).
20. Hansryd, J., Andrekson, P. A., Westlund, M., Li, J. & Hedekvist, P. O. Fiber-based optical parametric amplifiers and their applications. *IEEE J. Sel. Top. Quant. Electron.* **8,** 506–520 (2002).
21. Foster, M. A. *et al.* Broad-band optical parametric gain on a silicon photonic chip. *Nature* **441,** 960–963 (2006).
22. Tong, Z. *et al.* Towards ultrasensitive optical links enabled by low-noise phase-sensitive amplifiers. *Nature Photon.* **5,** 430–436 (2011).
23. Sweeny, M. & Mahler, R. A travelling-wave parametric amplifier utilizing Josephson junctions. *IEEE Trans. Magn.* **21,** 654–655 (1985).
24. Yurke, B., Roukes, M. L., Movshovich, R. & Pargellis, A. N. A low-noise series-array Josephson junction parametric amplifier. *Appl. Phys. Lett.* **69,** 3078–3080 (1996).
25. Parmenter, R. H. Nonlinear electrodynamics of superconductors with a very small coherence distance. *RCA Rev.* **23,** 323–352 (1962).
26. Anthore, A., Pothier, H. & Esteve, D. Density of states in a superconductor carrying a supercurrent. *Phys. Rev. Lett.* **90,** 127001 (2003).
27. Landauer, R. W. Superconductive parametric amplifier. US Patent 3,111,628 (1963).
28. Tholen, E. A. *et al.* Nonlinearities and parametric amplification in superconducting coplanar waveguide resonators. *Appl. Phys. Lett.* **90,** 253509 (2007).
29. Leduc, H. G. *et al.* Titanium nitride films for ultrasensitive microresonator detectors. *Appl. Phys. Lett.* **97,** 102509 (2010).
30. Mattis, D. C. & Bardeen, J. Theory of the anomalous skin effect in normal and superconducting metals. *Phys. Rev.* **111,** 412–417 (1958).
31. Pearl, J. Current distribution in superconducting films carrying quantized fluxoids. *Appl. Phys. Lett.* **5,** 65–66 (1964).
32. Anlage, S. M., Snortland, H. J. & Beasley, M. R. A current controlled variable delay superconducting transmission-line. *IEEE Trans. Magn.* **25,** 1388–1391 (1989).
33. Stolen, R. & Bjorkholm, J. Parametric amplification and frequency conversion in optical fibers. *IEEE J. Quant. Electron.* **18,** 1062–1072 (1982).
34. Landauer, R. Shock waves in nonlinear transmission lines and their effect on parametric amplification. *IBM J. Res. Dev.* **4,** 391–401 (1960).
35. Su, H. T., Wang, Y., Huang, F. & Lancaster, M. J. Superconducting delay lines. *J. Supercond.* **21,** 7–16 (2005).

Acknowledgements

The research was carried out at the Jet Propulsion Laboratory (JPL), California Institute of Technology, under a contract with the National Aeronautics and Space Administration and has been supported in part by NASA (Science Mission directorate), the Keck Institute for Space Studies, the Gordon and Betty Moore Foundation and the JPL Research and Technology Development program.

Author contributions

B.H.E. carried out the measurements and analysed the data. P.K.D. contributed to the device concept, designed the devices, planned the measurements, analysed the data and wrote the paper. H.G.L. developed the fabrication methods and made the devices. J.Z. contributed to the device concept and the writing of the paper.

Additional information

The authors declare no competing financial interests. Supplementary information accompanies this paper on www.nature.com/naturephysics. Reprints and permissions information is available online at www.nature.com/reprints. Correspondence and requests for materials should be addressed to P.K.D.